separations

MDPI

Article

Effective Removal of Hexavalent Chromium from Aqueous Solutions Using Quaternary Ammonium-Functionalized Magnetic Graphene Oxide Composites

Yue Huang [1,2,3], Weibin Huang [4], Ying Chen [1,5], Jianteng Sun [1,2,3], Maofeng Liang [1,5], Yonggui Guo [1,3,5], Xiaping Liu [1,3,5], Mingqiang Liu [1,3,5], Yajing Wei [1,5], Junfu Wei [1,3,5], Huan Zhang [1,2,3] and Huicai Wang [1,3,5,*]

1 State Key Laboratory of Separation Membranes and Membrane Processes, Tiangong University, Tianjin 300387, China
2 School of Environmental Science and Engineering, Tiangong University, Tianjin 300387, China
3 Cangzhou Institute of Tiangong University, Cangzhou 061000, China
4 Chongqing Key Laboratory of Agricultural Resources and Environment, College of Resources and Environment, Southwest University, Chongqing 400715, China
5 School of Chemical Engineering and Technology, Tiangong University, Tianjin 300387, China
* Correspondence: wanghuicai@tiangong.edu.cn

Abstract: Novel quaternary ammonium/magnetic graphene oxide composites (M-PAS-GO) that efficiently remove Cr(VI) ions were fabricated through the introduction of the (3-aminopropyl) triethoxysilane and Fe_3O_4 nanoparticles on the surface of GO, and then modified with n-butyl bromide. The fabricated M-PAS-GO was comprehensively characterized by SEM, TEM, EDX, XRD, Raman spectroscopy and FTIR, and the results manifest that the quaternary ammonium group was introduced onto the surface of GO. Under the reaction conditions of pH 3.20, temperature of 25 °C and M-PAS-GO dosage of 0.01 g/50 mL, 90% of 10 mg/L Cr(VI) ions were removed from the solution within 20 min. The kinetics study indicates that the adsorption process followed the pseudo-second-order model and was surface reaction-controlled. The thermodynamic parameters calculated from temperature-dependent adsorption isotherms suggest that the adsorption process was an exothermic and spontaneous process. The maximum adsorption capacities of Cr(VI) ions on M-PAS-GO composites calculated by the Langmuir model were 46.48 mg/g. Moreover, the reusability and stability of M-PAS-GO demonstrates its economic sustainability. This study suggests that M-PAS-GO is a potential candidate adsorbent for the separation of Cr(VI) from wastewater.

Keywords: quaternary ammonium groups; surface modification; magnetic graphene oxide; adsorption; hexavalent chromium

Citation: Huang, Y.; Huang, W.; Chen, Y.; Sun, J.; Liang, M.; Guo, Y.; Liu, X.; Liu, M.; Wei, Y.; Wei, J.; et al. Effective Removal of Hexavalent Chromium from Aqueous Solutions Using Quaternary Ammonium-Functionalized Magnetic Graphene Oxide Composites. *Separations* **2023**, *10*, 463. https://doi.org/10.3390/separations10090463

Academic Editor: Gavino Sanna

Received: 29 July 2023
Revised: 20 August 2023
Accepted: 22 August 2023
Published: 24 August 2023

1. Introduction

Environmental pollution by heavy metal ions is spreading globally along with industrial progress; in particular, mercury, lead, copper, cadmium and chromium are detected in wastewater from chemical manufacturing, painting and coating, mining, extractive metallurgy, nuclear and other industries, which can accumulate in organisms and poses a serious threat to ecosystems and human health through the food chain [1,2]. Among these heavy metal ions, Cr(VI) is of great concern due to its high toxicity, carcinogenicity, mutagenicity and wide application in industry [3]. Hence, it is critical to remove Cr(VI) from wastewater before it is discharged into water bodies. To date, a variety of methods have been developed to remove Cr(VI) from aqueous media, including adsorption, coagulation, membrane filtration, chemical oxidation, photodegradation and electrodialysis [4–8]. Among these methods, the adsorption process has been most widely employed because of its high availability, easy operability, low cost and high efficiency. Various materials, such as biomaterials, metal oxides [9], nanomaterials [10], activated carbon [11] and fibrous [12] and mesoporous inorganic sorbents [13–15] have been applied to remove Cr(VI) from

aqueous solutions. However, the adsorption ability of these materials for Cr(VI) in aqueous solution still need further improvement.

The application of nanomaterials in water treatment plants has attracted wide attention due to their advantages of large surface areas and more activated sites [16,17]. Since graphene was first identified through micromechanical exfoliation of graphite [18], many scientists have investigated it for various applications owing to its unusual mechanical, electrical and thermal properties. Graphene oxide (GO), prepared from graphite by the Hummers method, has been investigated as an efficient adsorbent for the removal of heavy metal ions and organic pollutants due to the presence of multiple active sites on its surface and the modification of many functional groups [19,20]. However, Cr(VI) exists mainly in anion form ($HCrO_4^-$, $Cr_2O_7^{2-}$, CrO_4^{2-}, etc.) in solution, and the low adsorption capacity of GO for Cr(VI) remains a major challenge due to its negatively charged surface. Safaviyan et al. [21] suggested the grafting of methacrylic acid onto magnetic graphene oxide (MGO) by radical polymerization and the attachment of tetraethylenepentamine (TEPA) to obtain an amino-rich adsorbent (MGOT), and its maximum adsorption capacity reached 287.15 mg/g under the optimal conditions. Other studies have also reported the modification of GO with metal compounds, and the adsorption properties of the modified GO were significantly enhanced [22–25].

Previous studies have shown that the removal efficiency of hexavalent chromium ions by adsorbents modified with amino and quaternary ammonium groups can be significantly improved: Xue et al. [26] reported a cellulose-based hyperbranched adsorbent (MCC/HBPA-0.88), which was prepared by cross-linking microcrystalline cellulose (MCC) and an amino-terminal grafted hyperbranched polymer ($HBPNH_2$), that achieved rapid and complete Cr(VI) removal in low-Cr(VI) water (1.02 mg/L) within 1 min. Liang et al. [10] synthesized a new cellulose-based adsorbent (PQC) modified with both quaternary ammonium salts and amino groups, which can remove Cr(VI) from solution under a wide range of pH levels. It was confirmed that the amino and quaternary ammonium groups on the adsorbent surface are the main adsorption sites [27], and adsorbents modified with these groups show efficient uptake under both acidic and basic conditions [28,29].

On the other hand, GO is difficult to separate from aqueous solution because of its small particle size, which can cause serious pollution once discharged into the environment [30]. For the recycling of GO materials, centrifugation is cumbersome, and filtration may lead to the clogging of filters. Compared with these traditional methods, magnetic separation is considered as an economic and effective technique for the recycling of nanomaterials from solution [31].

In this study, novel quaternary ammonium/magnetic graphene oxide composites (M-PAS-GO) were fabricated through the introduction of (3-aminopropyl) triethoxysilane and Fe_3O_4 nanoparticles on the surface of GO, followed by modification with n-butyl bromide. The surface morphology and crystalline phase of the M-PAS-GO composite were comprehensively characterized. The adsorption ability of the M-PAS-GO composite for Cr(VI), adsorption-influencing factors and the adsorption mechanism were investigated. Moreover, the recycling of the M-PAS-GO composite was also examined.

2. Materials and Methods

2.1. Chemicals and Materials

Graphite was purchased from Sigma-Aldrich. Sulfuric acid (95–98%), hydrogen chloride, nitric acid, 30% hydrogen peroxide, phosphorus pentoxide, potassium permanganate, sodium nitrate and 1.000 mg/mL Cr(VI) standard solution (prepared from its nitrate salts) were obtained from the Beijing Chemical Reagent Factory, along with (3-aminopropyl) triethoxysilane (APTES), carbodiimide (DCC), phosphate, sodium chloride (NaCl), ethanol, n-Butyl bromide, toluene and acetone. Cr(VI) metal ions under various pH conditions were obtained by directly diluting Cr(VI) standard solution with ultrapure water. All chemicals used in this study were of analytical grade, and were used without further

purification. All solutions were prepared with ultrapure water purified by a Millipore-Q system (18.2 MΩ cm).

2.2. Fabrication of Fe_3O_4 Nanoparticles

Fe_3O_4 nanoparticles were synthesized through the coprecipitation of Fe^{2+} and Fe^{3+} ions in ammonia solution and treatment under hydrothermal conditions [32,33]. Typically, 2.0 g of $Fe_3O_4 \cdot 7H_2O$ in 100 mL double-distilled water and 4.2 g of $FeCl_3 \cdot 6H_2O$ also in 100 mL ultrapure water were thoroughly mixed, and then added to 8 M NH_4OH under continuous stirring at 30 °C for 2 h. The precipitates were heated at 80 °C for 30 min, and the pH was maintained at 10 by adding NH_4OH. Impurity ions (i.e., chlorides and sulphates) were removed by washing with hot distilled water. The obtained Fe_3O_4 nanoparticles were sequentially washed with distilled water and ethanol several times, and then finally dried in a vacuum oven at 70 °C.

2.3. Synthesis of Quaternary Ammonium-Functionalized Magnetic Graphene Oxide Composite (M-PAS-GO)

The graphene oxide (GO) was obtained by the Hummers method through the oxidation of graphite powder [34]. In detail, 1.5 g of graphite powder was added to a concentrated H_2SO_4 (80 mL) solution at 0 °C. Meanwhile, 4.0 g of $KMnO_4$ was slowly added to the mixture under vigorous stirring, and the temperature was carefully controlled at 20 °C. Then, the mixture was stirred at 35 °C for 24 h, and diluted with distilled water. After that, 14 mL of 30% H_2O_2 solution was slowly added to the mixture until the color of the mixture changed to yellow. The mixture was purified by rinsing and centrifugation (10,000 rpm for 20 min) sequentially with 0.2 M HCl and distilled water several times. Finally, the solid GO was obtained after filtration and vacuum drying at 30 °C.

The amine-functionalized GO (APTES-GO) was synthesized by dispersing 100 mg of GO into 100 mL of toluene, and then adding 20 mL of APTES (2%) and magnetically stirring at 110 °C for 16 h. After centrifugation, the obtained APTES-GO was washed with toluene and acetone and then dried at 60 °C for 12 h.

The magnetic graphene oxide composite (M-APTES-GO) was synthesized according to the method reported in the literature [35]. Specifically, 100 mg of APTES-GO was added to 5 mL of buffer A (0.003 M phosphate, pH 6, 0.1 M NaCl), to which was then added 1.0 mL of carbodiimide solution, followed by sonication for 10 min (0.025 g/mL in buffer A). Then, 100 mg of Fe_3O_4 was dispersed into the mixture solution and then sonicated for 1 h in an ice bath. Finally, the obtained composites were washed thoroughly with ethanol and collected by using an external permanent magnet, and then dried in an oven at 60 °C.

Quaternary ammonium-functionalized magnetic graphene oxide composite (M-PAS-GO) was fabricated by dispersing 100 mg of M-APTES-GO into 100 mL of ethanol, and then adding 20 mL of n-butyl bromide under continuous stirring for 4 h at 90 °C. The composite materials were then collected magnetically from the suspension formed and washed with ethanol, and finally dried at 40 °C (see Scheme 1).

2.4. Analytical Methods

Transmission electron microscopy (TEM, H7650, Japan), scanning electron microscopy (SEM, Hitachi S-4800, Tokyo, Japan) and X-ray diffraction (XRD, Smartlab 9, Rigaku, Tokyo, Japan) were used to analyze the surface morphology and crystal structures of Fe_3O_4, GO and M-PAS-GO, respectively. A spectrophotometer (Nicolet 6700, Madison, WI, USA) was used to record the Fourier transform infrared (FT-IR) spectra of Fe_3O_4, GO and M-PAS-GO between 400 and 4000 cm^{-1} with a resolution of 2 cm^{-1}. A vibrating sample magnetometer (VSM, LakeShore7307, Quantum Design, San Diego, CA, USA) was used to determine the magnetic properties of Fe_3O_4 and M-PAS-GO at room temperature. The zeta potentials for a suspension of 0.5 g/L GO and M-PAS-GO in 0.1 M KNO_3 solution were determined using a Zetasizer Nano ZS90. Raman spectra were recorded with a Renishew Raman spectrometer. Brunauer–Emmett–Teller (BET) surface area was measured using the Micromeritics

ASAP 2010 at 77 K by N_2 adsorption–desorption isotherms. Thermogravimetric analysis (TGA) was recorded using a STA409PC DTA/TGA instrument (Netzsch, Bavaria, Germany) at a nitrogen flow rate of 50 mL/min in the temperature range of 25 °C to 800 °C at a rate of 10 °C/min. The concentrations of Cr(VI) were measured by ICP-OES (Perkin Elmer OptimaTM 2100 DV, PerkinElmer, Inc., Shelton, CT, USA).

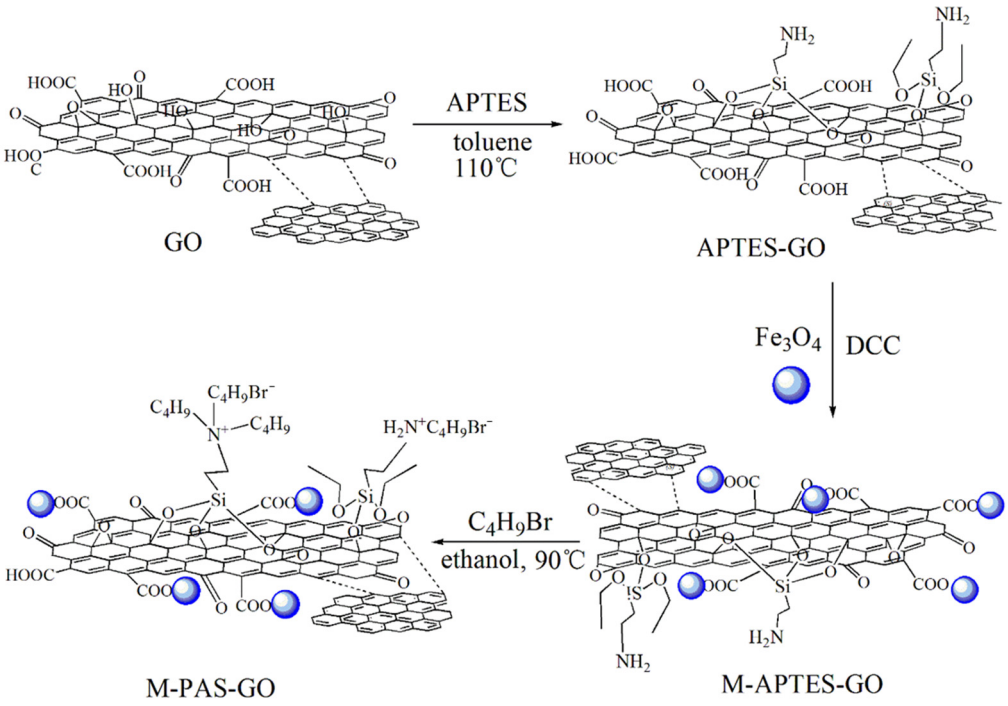

Scheme 1. Preparation process of the M-PAS-GO composite.

2.5. Batch Sorption Experiment

$K_2Cr_2O_7$ was used to prepare a Cr(VI) stock solution. All the sorption experiments were carried out according to the batch technique in a series of 50 mL conical bottles under continuous stirring of 200 r/min in a shaking water bath. The reaction solution was collected at 0 to 120 min during the adsorption process. Adsorption kinetics analysis and isotherm determination of Cr(VI) on M-PAS-GO composite were carried out at pH 3.20, and the initial concentrations of Cr(VI) ranged from 2.0 to 80.0 mg/L. The solution pH was adjusted with 0.1 M HCl and 0.1 M NaOH. After the suspensions were shaken for 24 h, the adsorbents were separated from the solution using a magnet. The concentrations of Cr(VI) in the filtrate were measured by ICP-OES. The amount of Cr(VI) adsorbed onto M-PAS-GO was calculated using Equation (1), and is expressed as the average ± standard deviation of three parallel experiments.

$$Q_e = \frac{(C_0 - C_e)V}{m} \quad (1)$$

where C_0 is the initial concentration (mg/L), C_e is the equilibrium concentration (mg/L), Q_e is the amount of Cr(VI) sorbed onto M-PAS-GO at the equilibrium time (mg/g), V is the solution volume (L) and m is the mass of the sorbent (g).

3. Results and Discussion

3.1. Characterization of the M-PAS-GO Composite

The surface morphologies of Fe_3O_4, GO and M-PAS-GO were observed by SEM and TEM. As shown in A1 and A2 of Figure 1, the Fe_3O_4 nanoparticles appear in spherical shape, with an average diameter of 20–30 mm. B1 and B2 of Figure 1 illustrate that the surface of the prepared GO is in the form of wrinkled fabric. C1 and C2 of Figure 1 clearly

show that Fe_3O_4 particles were successfully integrated with GO, and were well dispersed on the surface of the graphene nanosheets.

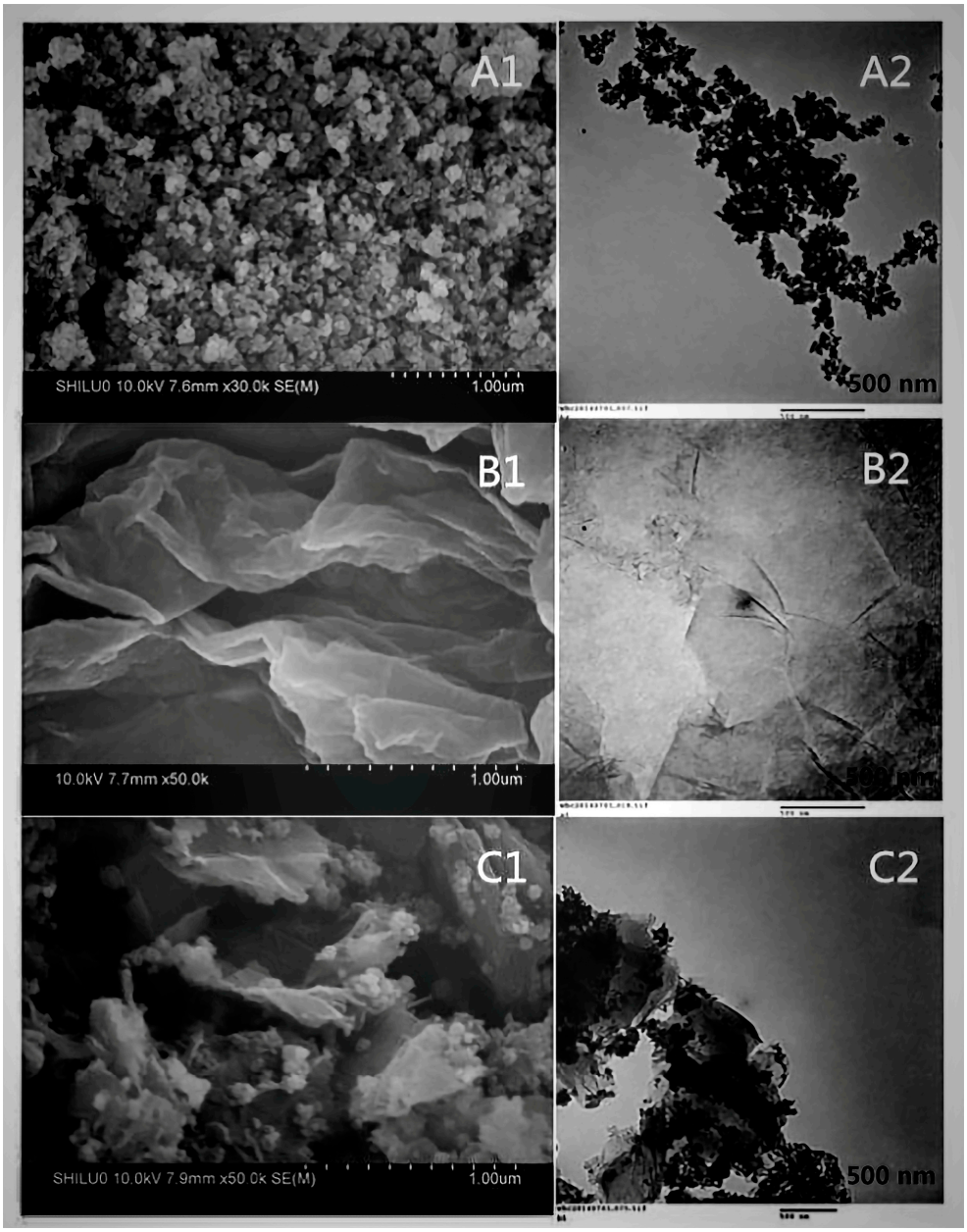

Figure 1. SEM and TEM images of (**A1**,**A2**) Fe_3O_4, (**B1**,**B2**) GO and (**C1**,**C2**) M-PAS-GO, respectively.

The XRD patterns of Fe_3O_4, GO and M-PAS-GO are shown in Figure 2a. The original graphite shows a sharp characteristic diffraction peak at 26.5°, as reported in previous work [36], corresponding to the (002) crystal plane. After the oxidation treatment, the (002) diffraction peak for graphite shifted to a lower angle of 10.5°, which is the graphene oxide (001) diffraction peak [37]. The main peaks at 30.2° (220), 35.7° (311), 43.3° (400), 53.7° (422), 57.4° (511) and 62.7° (440) represent the iron oxides in Fe_3O_4 and M-PAS-GO, respectively. These results are consistent with the standard profile of a cubic magnetite structure (JCPDS 65-3107) presented in a previous study [38]. It is interesting that no carbon peaks are observed in the XRD pattern of M-PAS-GO. This phenomenon may be attributed to the fact that the existence of Fe_3O_4 reduces the aggregation of the GO sheets, which results in more GO with fewer layers, and thus leads to weak peaks of carbon, or the strong signals of the iron oxides overwhelm the weak carbon peaks.

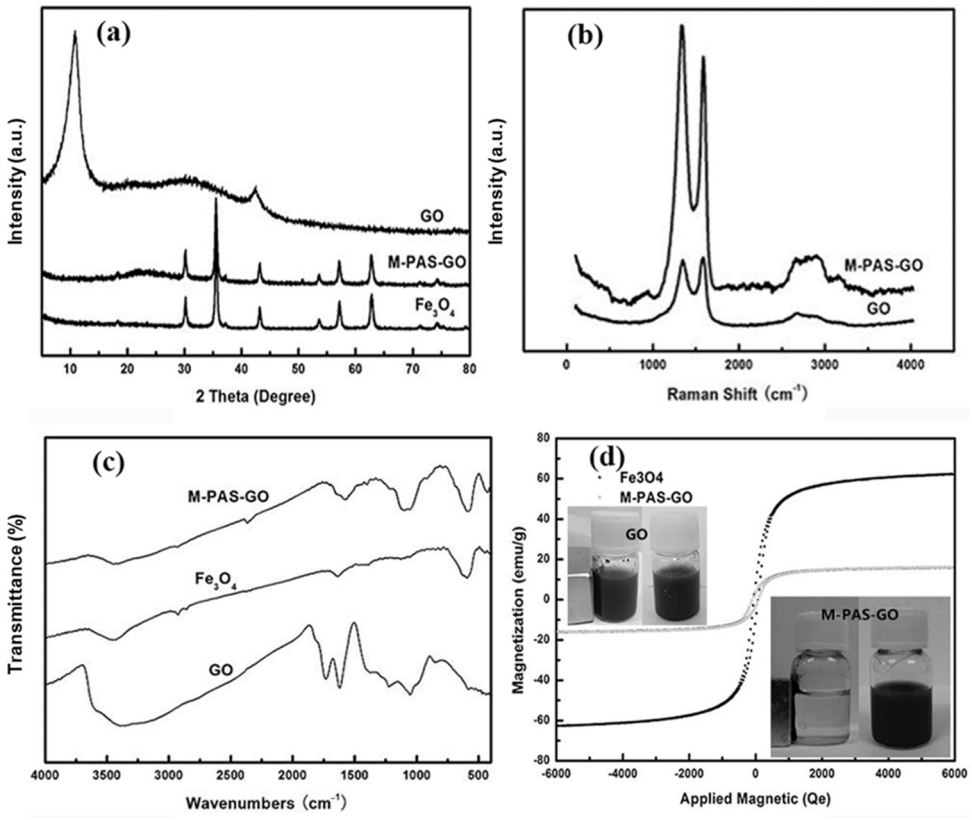

Figure 2. (**a**) XRD patterns of Fe_3O_4, GO and M-PAS-GO; (**b**) Raman spectra of GO and M-PAS-GO; (**c**) FT-IR spectra of Fe_3O_4, GO and M-PAS-GO; (**d**) magnetization curve of Fe_3O_4 and M-PAS-GO (insert photograph shows the magnetic responses of M-PAS-GO after and before adsorption).

Raman spectroscopy was employed to analyze the chemical bonding and structural changes in the carbon framework of the M-PAS-GO composite and GO, and the results are shown in Figure 2b. For both samples, the Raman spectra show two characteristic peaks between 1300 and 1600 cm^{-1}, which correspond to the D and G bands, respectively. According to a previous study [36], the D band corresponds to the disorder of GO originating from defects associated with vacancies, grain boundaries and amorphous carbon species, whereas the G band is ascribed to the first-order scattering of the E2g mode observed for sp^2 carbon domains. Compared with GO, the G and D bands of the M-PAS-GO composites shift to lower wave numbers, and the second-order features (2D band at 2652 cm^{-1} and (D + G) band at 2918 cm^{-1}) appear on the spectrum of the M-PAS-GO composites, indicating the reduction in GO. The intensity ratio of the D band to the G band (ID/IG) is very sensitive to the disordered structure of carbon. The ID/IG of M-PAS-GO composites obviously increased compared to that of GO, indicating the introduction of more numerous but smaller sp^2 carbon domains caused by the reduction in GO. The characteristic Raman band of Fe_3O_4 nanoparticles in the M-PAS-GO composite was found at about 610 cm^{-1}, ascribing to the A1g mode of Fe–O vibrations.

The FTIR spectra of the Fe_3O_4, GO, and M-PAS-GO are shown in Figure 2c. The peaks at 1730, 1625 and 1100 cm^{-1} were observed in the spectrum of GO, which correspond to stretching of the C=O bond of carboxyl groups, the vibrations of skeletal C=C in GO and alkoxy C-O, respectively [39]. The new peak at 575 cm^{-1} was observed in the FTIR spectrum of M-PAS-GO, which differs from that of GO and is consistent with that of Fe_3O_4, thus can be related to the vibration of Fe-O functional groups [40]. Moreover, peaks at 1625 cm^{-1} and 1147 cm^{-1} which related to the C=O and C-N group, respectively, was also observed in this study. These findings indicates that the Fe_3O_4 and quaternary ammonium group were successfully modified onto the surface of GO. In addition, the characteristic peaks in 2900 cm^{-1} in the spectra of Fe_3O_4 and M-PAS-GO suggest the presence of unsaturated

groups, which bring the prepared material more binding sites on its surface and thus enhance their adsorption capacities [41].

The magnetization hysteresis loops of Fe_3O_4 and M-PAS-GO at room temperature are illustrated in Figure 2d. It can be seen that the saturation magnetization of the obtained Fe_3O_4 and M-PAS-GO is about 62.4 emu/g and 18.1 emu/g, respectively. This result indicates that the M-PAS-GO composite possessed excellent magnetic properties. As can be seen in the insert photograph of Figure 2d, without an external magnetic field, a black homogeneous dispersion emerged. This phenomenon further confirms that M-PAS-GO is magnetic and can be used as a magnetic adsorbent to enrich contaminants adsorbed from bulk aqueous solutions.

The zeta potentials of the M-PAS-GO and GO magnetic nanoparticles in aqueous solutions with different pH were measured, as shown in Figure 3a. It is clear that the zeta potentials of M-PAS-GO and GO decreased with the increase in pH from 1 to 8. The zeta potential of GO was negative at the entire pH range, whereas the pH_{zpc} (zero point charge) of M-PAS-GO magnetic composites is about 4.0. These results indicate that when pH is lower than 4, M-PAS-GO is more favorable for adsorption of surface negatively charged pollutants compared to GO.

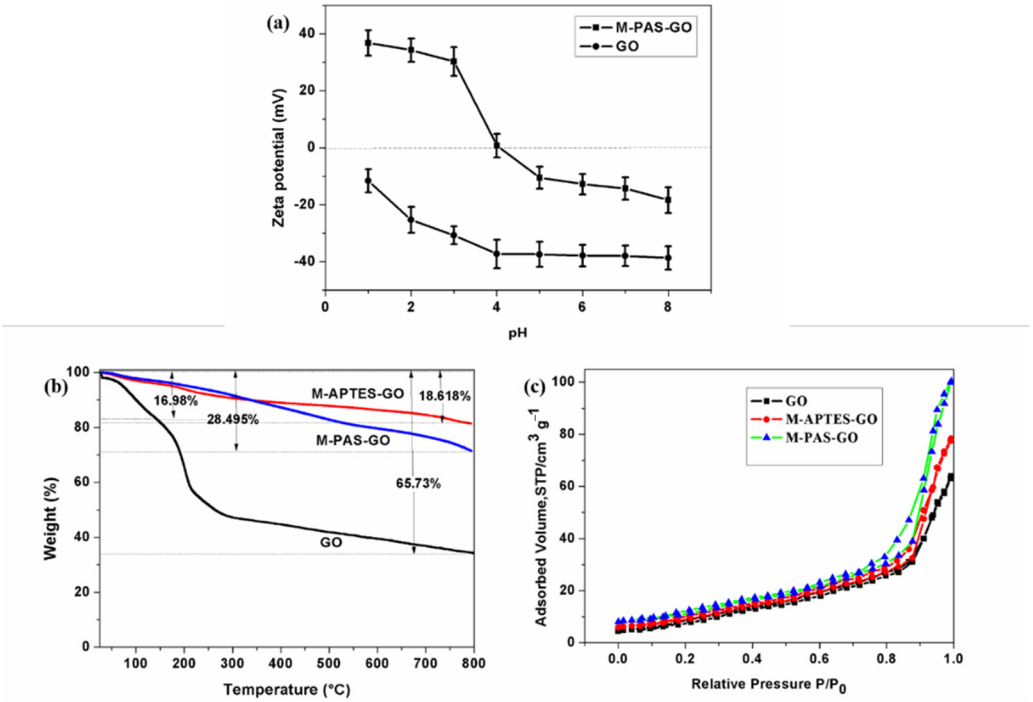

Figure 3. (**a**) Zeta potential of GO and M-PAS-GO; (**b**) TGA curves of GO, M-APTES-GO and M-PAS-GO composites; (**c**) BET of GO, M-APTES-GO and M-PAS-GO composites.

Figure 3b shows the TGA curves of GO, M-APTES-GO and M-PAS-GO composites. The dramatic weight loss of 65.73 % in GO was observed when the temperature increased from 30 to 800 °C, which can be attributed to the thermal decomposition of oxygen containing groups (such as –OH, –COOH, –O– and C=O) [42]. Meanwhile, the thermal degradation of M-APTES-GO and M-PAS-GO composites was observed and the loss was 18.618% and 28.495% when the temperature increased to 800 °C, respectively, which is caused by the reduction in APTES, quaternary ammonium group and Fe_3O_4 nanoparticles. Compared with M-APTES-GO, an additional weight loss of 9.877% was found in M-PAS-GO, which proves that there were 9.877% of the quaternary ammonium group in M-APTES-GO composites, and further proves that the preparation of quaternary ammonium group functionalized magnetic composites is successful.

The BET pattern of GO, M-APTES-GO and M-PAS-GO composites as shown in Figure 3c. According to the N_2 adsorption analysis, the BET surface areas of GO and M-APTES-GO are 62.28 cm^2/g and 78.44 cm^2/g, respectively. A significant increase in BET surface area to 102.24 cm^2/g was found in M-PAS-GO, which may be beneficial for its pollutant adsorption performance.

Combining with the characterizations and adsorption experiments, the EDX patterns of GO and M-PAS-GO before and after adsorption experiments are illustrated in Figure 4. The results show that the surface of M-PAS-GO exhibits high content of Fe (4.28%), N (4.05%) and Si (4.32%), indicating that Fe_3O_4 nanoparticles and quaternary ammonium groups were successfully introduced into graphene oxide. After adsorption experiment, the content of Cr on the surface of M-PAS-GO was 1.02%, and that on GO was negligible (0.002%), which shows the excellent adsorption ability of M-PAS-GO.

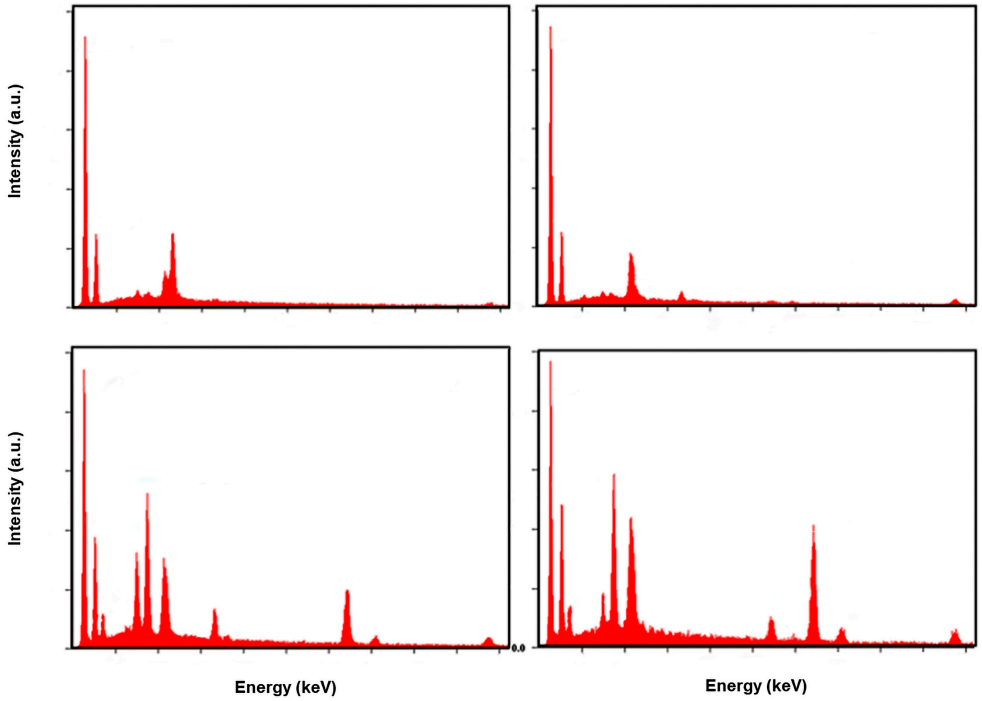

Figure 4. EDX patterns of GO, GO-Cr, M-PAS-GO and M-PAS-GO-Cr.

3.2. Effect of pH on Cr(VI) Adsorption by M-PAS-GO Composite

The pH of the solution can affect the ionization and the speciation of metal ions, and the surface properties of quaternary ammonium composite. At low pH condition (pH 1–6), $HCrO_4^-$ and $Cr_2O_7^{2-}$ are the main species in solution, while the main specie transforms to CrO_4^{2-} at the pH 6–10 [23]. The effect of solution pH on Cr(VI) ions adsorption was investigated, and the results are shown in Figure 5a, and the change in pH value before and after adsorption is shown in Figure 5b. It can be seen that the M-PAS-GO composite shows high equilibrium adsorption level (Q_e > 35 mg/g) for Cr(VI) (i.e., $HCrO_4^-$ and $Cr_2O_7^{2-}$) at pH 2.10–3.20. However, the adsorption level of Cr(VI) (i.e., $HCrO_4^-$, $Cr_2O_7^{2-}$ and CrO_4^{2-}) decreases with the increase in pH from 3.20 to 8.00. These trends are related to anionic forms and the surface properties of the M-PAS-GO composite. As analyzed in Figure 3, the pH_{zpc} of M-PAS-GO is 4.00, which makes the surface of M-PAS-GO positively charged at pH < 4.00 and negatively charged at pH > 4.00. Thus, at low pH conditions (pH < 4.00), $HCrO_4^-$ and $Cr_2O_7^{2-}$ were adsorbed onto positive sites via electrostatic binding; thus, the high adsorption level of the M-PAS-GO composite was achieved. When the pH > 4.0, the main specie in solution is CrO_4^{2-} and the surface of M-PAS-GO becomes negatively charged, which leads to the enhancement of the repulsion between the M-PAS-GO and CrO_4^{2-}. In addition, the competitive adsorption between OH^- and CrO_4^{2-} and the

formation of hydroxyl complexes of chromium may also inhibit the adsorption of Cr(VI) ions. Therefore, the appropriate pH was selected as 3.20.

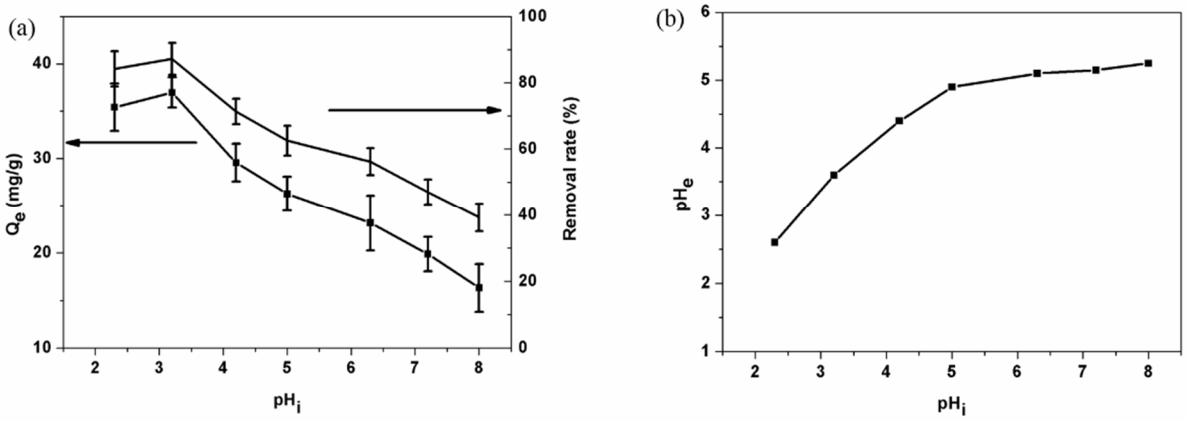

Figure 5. (**a**) The effect of initial pH on adsorption of Cr(VI) onto M-PAS-GO; (**b**) changes in pH value before and after adsorption.

3.3. Effect of M-PAS-GO Dosage on Cr(VI) Adsorption

The effect of M-PAS-GO dosage on Cr(VI) (i.e., $HCrO_4^-$ and $Cr_2O_7^{2-}$) adsorption was investigated under the conditions of pH 3.20, temperature of 25 °C and initial Cr(VI) concentration of 10 mg/L, and the results are shown in Figure 6. It can be seen that the removal efficiency of Cr(VI) ions increases sharply from 17% to 86% when the adsorbent dosage increased from 0.002 to 0.01 g/50 mL, then a slight decrease occurred, and then a negligible increase in Cr(VI) ion removal was observed when the adsorbent dosage further increased to 0.012 g/50 mL and 0.016 g/50 mL, respectively. Meanwhile, the adsorption level of the M-PAS-GO composite decreased from 46.4 to 22.5 mg/g with the increase in its dosage. This may be because an adsorbent with a higher dosage can increase the number of active adsorption sites. However, aggregation occurs due to the magnetic properties of the M-PAS-GO composite, leading to a decrease in its specific surface area, which in turn leads to a decrease in the adsorption sites and then a decrease in the adsorption ability; additionally, an increase in the mass of aggregated M-PAS-GO results in its precipitation, which is also not conducive to the adsorption of pollutants [43]. Considering the removal efficiency for Cr(VI) ions and the adsorption level of M-PAS-GO, the optimal adsorbent dosage was selected as 0.01 g/50 mL for the subsequent experiments.

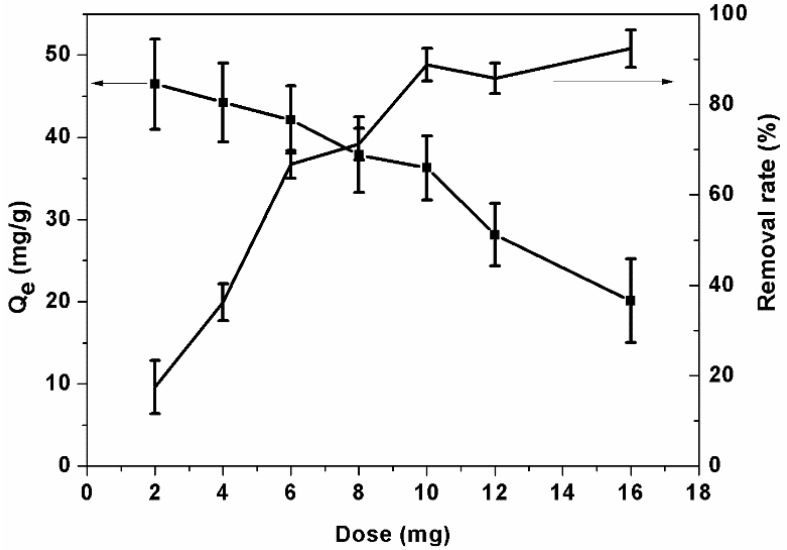

Figure 6. Effect of dosage of M-PAS-GO on Cr(VI) removal.

3.4. Effect of Contact Time on Cr(VI) Adsorption by M-PAS-GO

To study the absorption kinetics, the adsorption levels of M-PAS-GO for Cr(VI) (i.e., $HCrO_4^-$ and $Cr_2O_7^{2-}$) at different contact times were calculated. The reaction conditions were as follows: Cr(VI) concentration of 10 mg/L, pH of 3.20, adsorbent dosage of 0.01 g/50 mL and temperature of 25 °C. As described in Figure 7a, a sharp increase in Cr(VI) adsorption occurred in the first 15 min, and stabilized in the subsequent times. In the study of [44], the removal efficiency of 10 mg/L Cr(VI) by phytogenic zero-valent iron nanoparticles was only ~20% in 20 min. Liu et al. [45] used a magnetic zeolite/chitosan composite adsorbent and achieved less than 70% removal of 10 mg/L Cr(VI) within 30 min. It is noteworthy that in this study, 90% of the 10 mg/L Cr(VI) ions were adsorbed within 20 min, and saturation was achieved in 30 min, with the result of 46.48 mg/g of Cr(VI) ions being removed by M-PAS-GO, which is higher than the removal achieved by the other materials listed in Table 1. These results indicate the excellent adsorption ability of M-PAS-GO, which can be attributed to the large number of quaternary ammonium groups on its surface that can interact with Cr(VI) ions.

Table 1. Comparison of adsorption capacities for Cr(VI) of different adsorbents.

Adsorbents	pH	q_m (mg/g)	Ref.
Phytogenic zero-valent iron nanoparticles	4.3–10.0	9.0	[44]
Separable magnetic zeolite/chitosan composite (MZFA/CS)	3.0	16.96	[45]
Ion-imprinted adsorbent material	2.5	2.4	[46]
PI-PEI	2.0–6.0	44.67	[47]
Mg-Al-LDH	1.75–6.0	38.9	[48]
Fe(III)–chitosan microbeads (Fe-CTB)	3.0	34.15	[49]
M-PAS-GO	3.20	46.48	This work

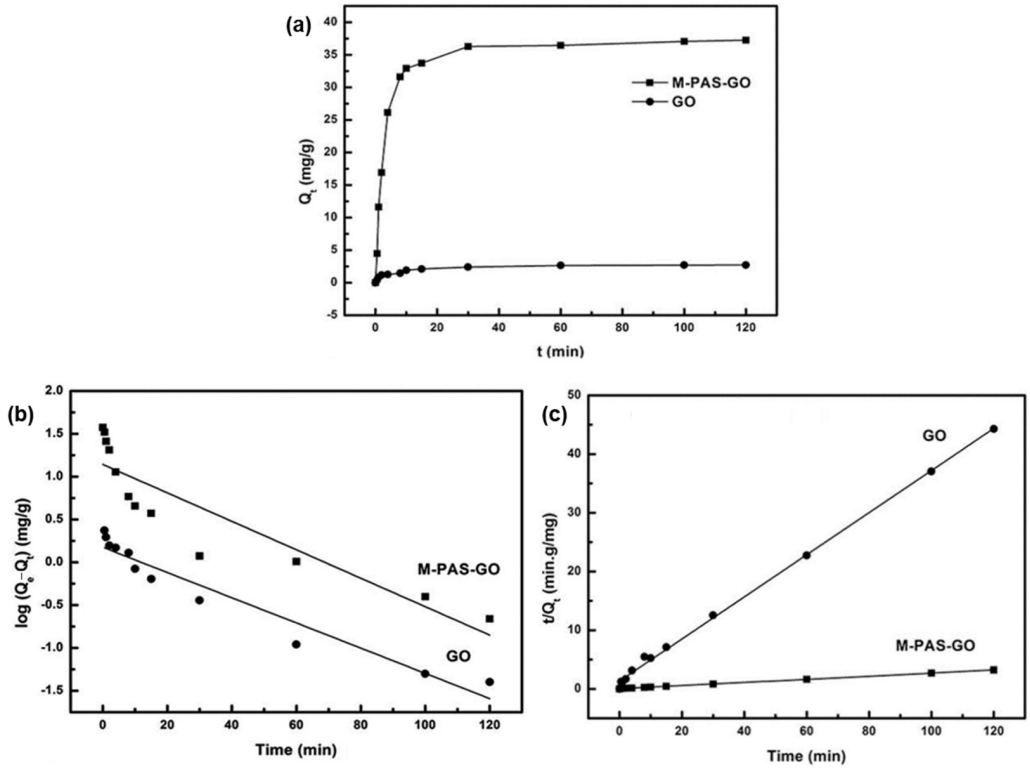

Figure 7. (**a**) Effect of contact time on the adsorption capacity of GO and M-PAS-GO; (**b**) pseudo-first-order kinetic plots for adsorption of GO and M-PAS-GO; (**c**) pseudo-second-order kinetic plots for adsorption of GO and M-PAS-GO.

The pseudo-first-order and pseudo-second-order models were employed to analyze the experimental kinetic data according to the following linear equations.

Pseudo-first-order model:

$$\log(Q_e - Q_t) = \log Q_e - \left(\frac{k_1 t}{2.303}\right) \tag{2}$$

Pseudo-second-order model:

$$\frac{t}{Q_t} = \frac{1}{k_2 Q_e^2} + \frac{1}{Q_e} t \tag{3}$$

where k_1 (min^{-1}) and k_2 (g/(mg·min)) are the pseudo-first-order rate constant and pseudo-second-order kinetic rate constant, respectively, and Q_e and Q_t are the adsorption level (mg/g) of the adsorbent for metal ions at equilibrium and at contact time t (min), respectively.

The linear fitting and the correlation coefficient of the pseudo-first-order and pseudo-second-order equations for the adsorption of Cr(VI) ions by M-PAS-GO are shown in Figure 7b,c and Table 2. The results indicate that the pseudo-second-order model is more suitable for describing the adsorption behavior of Cr(VI) ions when using GO and M-PAS-GO ($R^2 > 0.99$), which suggests that the rate-limiting step of adsorption is a chemisorption between the metals ions and binding sites of the M-PAS-GO and GO [13,14]. Therefore, it can be inferred that the adsorption of Cr(VI) on M-PAS-GO is mainly controlled by the chemical interaction between adsorbents and Cr(VI) ions.

Table 2. The kinetics models for the adsorption of Cr(VI) onto GO and M-PAS-GO.

Model	Parameter	GO	M-PAS-GO
Pseudo-first-order model	Q_{exp} (mg/L)	2.75	37.47
	Q_{1cal} (mg/g)	1.4969	13.8810
	k_1 (min^{-1})	0.0339	0.03823
	R^2	0.9382	0.8074
Pseudo-second-order model	Q_{2cal} (mg/g)	2.7896	37.8072
	k_2 (g/(mg·min))	0.0955	0.0142
	h (mg/(g·min))	0.7434	20.3417
	R^2	0.9980	0.9995

3.5. Effect of Initial Concentration on Cr(VI) Adsorption by M-PAS-GO

The adsorption isotherms of Cr(VI) (i.e., $HCrO_4^-$ and $Cr_2O_7^{2-}$) by M-PAS-GO were investigated. The reaction conditions were as follows: pH of 3.20, temperature of 25 °C, adsorbent dosage of 0.01 g/50 mL and contact time of 120 min. The results in Figure 8 illustrate that, initially, the isotherm rises sharply with the increase in the equilibrium concentrations, which may be attributed to the fact that plenty of adsorption sites are available for Cr(VI) ions. Then, the adsorption process gradually reaches saturation with the increase in initial Cr(VI) concentration, and no more available adsorption sites remain. In order to further study the interaction between the Cr(VI) ions and the adsorbents, Langmuir, Freundlich and Temkin adsorption models were used to fit the isothermal adsorption data, and the fitting parameters are given in Table 3. The equations for the isotherm models of Langmuir, Freundlich and Temkin are as follows:

$$Q_e = \frac{Q_m b C_e}{1 + b C_e} \tag{4}$$

$$Q_e = K_f C_e^{1/n} \tag{5}$$

$$Q_e = \frac{RT}{b} \ln A + \frac{RT}{b} \ln C_e \tag{6}$$

where Q_e and Q_m (mg/g) are the equilibrium and theoretical saturated adsorption capacities of the adsorbent in the monolayer cover layer, respectively; b represents the equilibrium constant of the adsorption reaction (L/mg); C_e (mg/L) is the concentration of Cr(VI) at equilibrium; K_f and n are the Freundlich constants, which are related to the adsorption capacity of the adsorbent and adsorption intensity; $1/n$ is a heterogeneous factor that is related to the adsorption strength and favorability; R (8.3145 J/(mol·K)) is the gas constant; T (K) is the temperature; b (J·mol) is the Temkin constant related to the heat of adsorption; A (L/g) is the equilibrium binding constant.

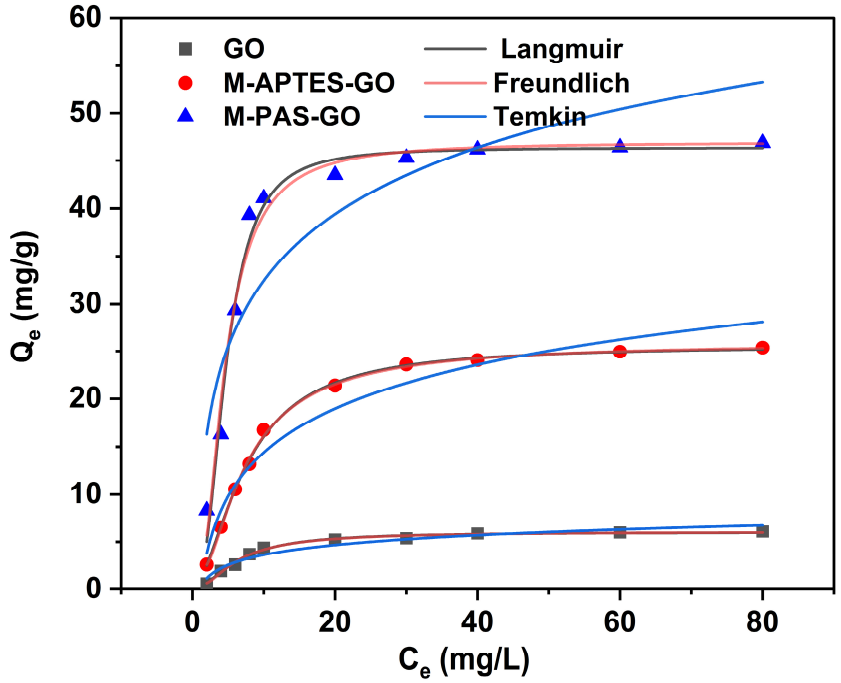

Figure 8. Adsorption isotherm of Cr(VI) on GO M-APTES-GO and M-PAS-GO at 298 K.

Table 3. A comparison of the results of three isotherm models for Cr(VI) adsorption on GO and M-PAS-GO.

Model	Parameter	GO	M-APTES-GO	M-PAS-GO
Langmuir	q_m (mg/g)	5.67	24.65	46.48
	b(L/mg)	0.0496	1.2495	1.5288
	R^2	0.9571	0.9913	0.9735
Freundlich	K_f(L/g)	0.654	12.584	24.013
	n	2.1953	4.2513	5.5172
	R^2	0.9255	0.9892	0.9311
Temkin	A(L/mg)	0.6171	46.2513	125.5374
	B	1.1511	4.1564	5.4697
	R^2	0.9480	0.9586	0.9600

As can be seen in Table 3, the R^2 values of the three isotherm models are higher than 0.9, indicating that they are well-fitted to the adsorption processes. The relatively high R^2 obtained with the Langmuir model indicates that the adsorption is a monolayer adsorption process. These results are similar to those of other studies on the adsorption of Cr(VI) using quaternary ammonium-modified adsorbents [10,28]. Calculated by Langmuir adsorption model, the saturated adsorption levels of Cr(VI) on M-APTES-GO and M-PAS-GO were 24.65 mg/g and 46.48 mg/g, which are four and eight times as much as that of GO (5.67 mg/g), respectively. The excellent adsorption ability of M-PAS-GO can be attributed to its large and positively charged surface (see Figure 3a,c), which promotes

electrostatic interactions between M-PAS-GO and anions (i.e., $HCrO_4^-$ and $Cr_2O_7^{2-}$) in solution. In the Freundlich isotherm, *n* values between 1 and 10 are generally favorable for adsorption [3]. As shown in Table 3, the *n* values lie between 1 and 10 for Cr(IV), suggesting that the use of GO, M-APTES-GO and M-PAS-GO as adsorbents favors the adsorption of Cr(IV) in solution. The adsorption process of Cr(VI) in this study was also well-fitted in the Temkin isotherm model, which assumes that the free energy of adsorption per layer decreases linearly with increasing adsorbate on the adsorbent surface due to adsorbate and adsorbate–adsorbent interactions rather than in a logarithmic form [45].

3.6. Effect of Temperature on Cr(VI) Adsorption by GO and M-PAS-GO

The effect of temperature on the adsorption of Cr(VI) (i.e., $HCrO_4^-$ and $Cr_2O_7^{2-}$) by fabricated adsorbents was also investigated. The adsorption conditions were as follows: different temperature conditions, including 298 K, 308 K, 318 K and 328 K, different initial concentrations, including C_0 = 2, 6, 10, 20 and 30 mg/L, adsorbent dosage of 0.01 g/50 mL, pH of 3.20 and contact time of 120 min. Further, the adsorption thermodynamic behavior was studied via different thermodynamic parameters (i.e., Gibb's free energy (ΔG°), entropy (ΔS°) and enthalpy (ΔH°)), which were calculated through the following equation:

$$\Delta G^\circ = -\mathrm{RT}\ln K_c \tag{7}$$

$$K_c = \frac{Q_e}{C_e} \tag{8}$$

The standard enthalpy change (ΔH°) and the standard entropy (ΔS°) were then obtained from the linear plot of lnK_c versus 1/T for Cr(VI) ion adsorption on the GO and M-PAS-GO composites in the following equation:

$$\ln K_c = \frac{\Delta S^\circ}{R} - \frac{\Delta H^\circ}{RT} \tag{9}$$

As illustrated in Figure 9a, when the concentrations of Cr(VI) were 2 and 6 mg/L, no obvious difference was found in the adsorption capacity of M-PAS-GO in the temperature range of 298–328 K. Meanwhile, a decrease in the adsorption capacity of M-PAS-GO was observed with increasing temperature when the Cr(VI) concentrations were 10, 20 and 30 mg/L, meaning that the adsorption process is exothermic. The thermodynamic curves of M-PAS-GO and GO for the adsorption of 20 mg/L Cr(VI) at 298–328 K are shown in Figure 9b,c, and the calculated ΔH° and ΔG° values are given in Table 4. The results show that when using M-PAS-GO, ΔG° is negative and gradually increases with the increase in temperature, indicating that the adsorption process is spontaneous, and that the elevated temperature would reduce the adsorption capacity of the adsorbent for Cr(VI) ions [3], which is further demonstrated by the results in Figure 9a. In contrast, ΔG° is positive when using GO, suggesting that the adsorption process is non-spontaneous, and further explaining the low adsorption efficiency. This phenomenon may be caused by the electrostatic repulsion between the negatively charged GO surface (see Figure 3a) and the anions (i.e., $HCrO_4^-$ and $Cr_2O_7^{2-}$). The obtained negative value of ΔH° can be explained by the fact that Cr(VI) adsorption is an exothermic process, which is consistent with the results in Figure 9a. The obtained negative value of ΔS° reveals that the adsorption of Cr(VI) ions by M-PAS-GO is a process of transition from randomness in solution to relative order on a solid surface [3].

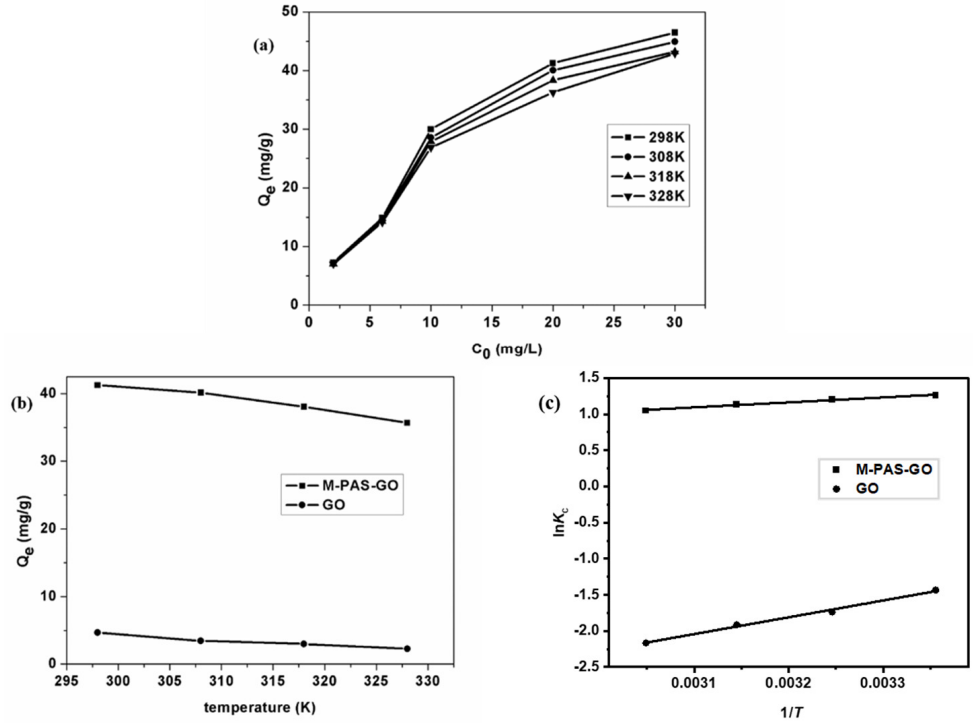

Figure 9. (**a**) Adsorption isotherms of Cr(VI) at different temperatures onto M-PAS-GO composites; (**b**) the effect of temperature on Cr(VI) adsorption by GO and M-PAS-GO composites (C_0 = 20 mg/L); (**c**) adsorption thermodynamics of Cr(VI) adsorption on GO and M-PAS-GO composites.

Table 4. Thermodynamic parameters for the adsorption of Cr(VI) on GO and M-PAS-GO composites.

Adsorbents	ΔG°_{ads} (kJ/mol)				ΔH°_{ads} (kJ/mol)	ΔS°_{ads} (J/(mol·k))
	298 K	308 K	318 K	328 K		
GO	3.59	4.36	5.13	5.90	−19.33	−76.90
M-PAS-GO	−3.15	−3.06	−2.98	−2.89	−5.70	−8.56

3.7. Regeneration and Reuse of Adsorbents

The M-PAS-GO composite exhibits excellent adsorption performance in terms of Cr(VI) (i.e., $HCrO_4^-$ and $Cr_2O_7^{2-}$); whether it can keep good stability and reusability is crucial for its large-scale application. Therefore, a desorption experiment was conducted, in which 0.05 g of M-PAS-GO, after the adsorption process, was subjected to 25 mL of 0.1 M NaOH and ultrasonicated for 120 min. The results show that there was only a 7.85% loss of Fe element observed in the filtrate, indicating that the M-PAS-GO composite had an acceptable regeneration property. Moreover, five consecutive adsorption–desorption cycles were conducted, the results of which are illustrated in Figure 10. These results demonstrate that the adsorption capacity of M-PAS-GO decreased from 46.14 to 33.41 mg/g at the fifth adsorption–desorption cycle, which may be attributed to the fact that the adsorbed Cr(VI) ions were not completely released from the adsorption sites, and the sight loss of the adsorbent during the regeneration processes. Nevertheless, M-PAS-GO maintained a high adsorption capacity, and the Cr(VI) ions in solution were removed completely. These results indicate that M-PAS-GO has promising reusability and stability, and can be a potential adsorbent in practical environmental remediation.

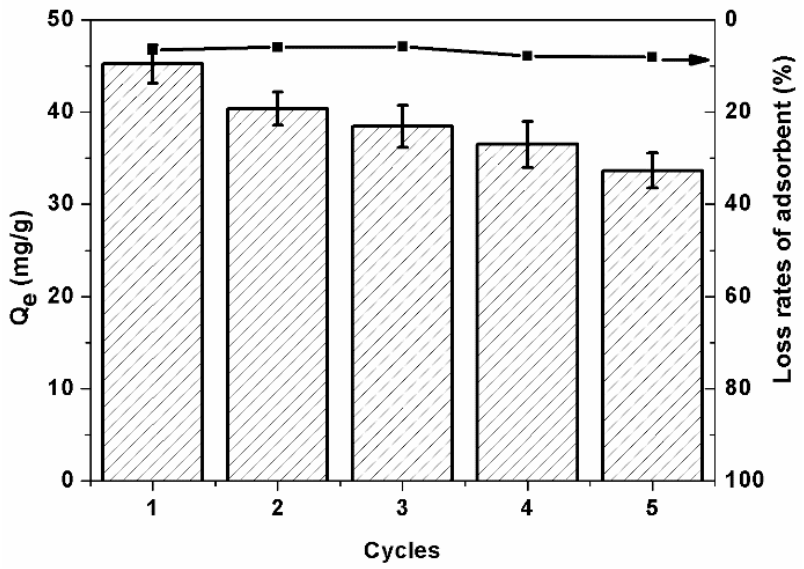

Figure 10. Cr(VI) adsorption on regenerated M-PAS-GO adsorbent and the loss rates of adsorbent with five adsorption–regeneration cycles at 298 K.

4. Conclusions

In summary, a quaternary ammonium/magnetic graphene oxide composite (M-PAS-GO) based on Fe_3O_4 bonded to the surface of 3-aminopropyltriethoxysilane (APTES) functional graphene oxide, and then modified with n-butyl bromide, has been successfully fabricated. Notably, a high surface potential, a surface area of 102.24 cm^2/g and an adsorption capacity of 46.48 mg/g for Cr(VI) ions were obtained by the M-PAS-GO composite. The effects of adsorbent dosage, solution pH, contact time, initial concentration of Cr(VI) ions and temperature on the adsorption process were comprehensively investigated. When using M-PAS-GO, a satisfying removal efficiency of Cr(VI) ions was achieved, namely, 90% within 10 min under optimal conditions, which can be attributed to the large number of quaternary ammonium groups on its surface that can interact with Cr(VI) ions. The mechanistic studies demonstrated that the adsorption is surface reaction-controlled, and is an exothermic and spontaneous process. In addition, the M-PAS-GO composite exhibited excellent reusability and stability. This study suggests that M-PAS-GO can be used as a potential adsorbent for the removal of Cr(VI) from wastewater, and provides referential support for further quaternary ammonium-modified adsorbent investigation.

Author Contributions: Y.H.: Methodology, Investigation, Data curation, Writing—original draft, Writing—Reviewing and Editing. W.H.: Methodology, Investigation, Writing—Reviewing and Editing. Y.C.: Methodology, Investigation. J.S.: Methodology, Investigation. Y.G.: Methodology, Investigation. M.L. (Maofeng Liang): Methodology, Investigation. X.L.: Methodology, Investigation. M.L. (Mingqiang Liu): Methodology, Investigation. Y.W.: Methodology, Investigation. J.W.: Supervision. H.Z.: Supervision. H.W.: Supervision, Conceptualization, Funding acquisition, Writing—Reviewing and Editing. All authors have read and agreed to the published version of the manuscript.

Funding: This research was funded by the Science and Technology Plans of Tianjin (No: 22YFX-THZ00040), the research funding provided by Cangzhou Institute of Tiangong University (No. TGCYY-F-0207), the TGU Grant for Fiber Studies (Grant No: TGF-21-A7), the Undergraduate Innovation and Entrepreneurship Training Program of Tiangong University (202110058051).

Data Availability Statement: All data generated or analyzed during this study are included in this published article.

Conflicts of Interest: The authors declare no conflict of interest.

References

1. Zaynab, M.; Al-Yahyai, R.; Ameen, A.; Sharif, Y.; Ali, L.; Fatima, M.; Khan, K.A.; Li, S. Health and environmental effects of heavy metals. *J. King Saud Univ. Sci.* **2022**, *34*, 101653. [CrossRef]
2. Briffa, J.; Sinagra, E.; Blundell, R. Heavy metal pollution in the environment and their toxicological effects on humans. *Heliyon* **2020**, *6*, e04691. [CrossRef] [PubMed]
3. Wang, H.; Wang, Z.; Yue, R.; Gao, F.; Ren, R.; Wei, J.; Wang, X.; Kong, Z. Rapid preparation of adsorbent based on mussel inspired chemistry and simultaneous removal of heavy metal ions in water. *Chem. Eng. J.* **2020**, *383*, 123107. [CrossRef]
4. Mondal, S.; Majumder, S.K. Fabrication of the polysulfone-based composite ultrafiltration membranes for the adsorptive removal of heavy metal ions from their contaminated aqueous solutions. *Chem. Eng. J.* **2020**, *401*, 126036. [CrossRef]
5. Zhou, H.; Zhu, H.; Xue, F.; He, H.; Wang, S. Cellulose-based amphoteric adsorbent for the complete removal of low-level heavy metal ions via a specialization and cooperation mechanism. *Chem. Eng. J.* **2020**, *385*, 123879. [CrossRef]
6. Wu, S.; Dai, X.; Kan, J.; Shilong, F.; Zhu, M. Fabrication of carboxymethyl chitosan–hemicellulose resin for adsorptive removal of heavy metals from wastewater. *Chin. Chem. Lett.* **2017**, *28*, 625–632. [CrossRef]
7. Castro-Riquelme, C.L.; López-Maldonado, E.A.; Ochoa-Terán, A.; Alcántar-Zavala, E.; Trujillo-Navarrete, B.; Pérez-Sicairos, S.; Miranda-Soto, V.; Zizumbo-López, A. Chitosan-carbamoylcarboxylic acid grafted polymers for removal of metal ions in wastewater. *Chem. Eng. J.* **2023**, *456*, 141034. [CrossRef]
8. Malik, L.A.; Bashir, A.; Qureashi, A.; Pandith, A.H. Detection and removal of heavy metal ions: A review. *Environ. Chem. Lett.* **2019**, *17*, 1495–1521. [CrossRef]
9. Liu, N.; Zhang, Y.; Xu, C.; Liu, P.; Lv, J.; Liu, Y.; Wang, Q. Removal mechanisms of aqueous Cr(VI) using apple wood biochar: A spectroscopic study. *J. Hazard. Mater.* **2020**, *384*, 121371. [CrossRef]
10. Liang, X.; Liang, B.; Wei, J.; Zhong, S.; Zhang, R.; Yin, Y.; Zhang, Y.; Hu, H.; Huang, Z. A cellulose-based adsorbent with pendant groups of quaternary ammonium and amino for enhanced capture of aqueous Cr(VI). *Int. J. Biol. Macromol.* **2020**, *148*, 802–810. [CrossRef]
11. Kharrazi, S.M.; Soleimani, M.; Jokar, M.; Richards, T.; Pettersson, A.; Mirghaffari, N. Pretreatment of lignocellulosic waste as a precursor for synthesis of high porous activated carbon and its application for Pb (II) and Cr (VI) adsorption from aqueous solutions. *Int. J. Biol. Macromol.* **2021**, *180*, 299–310. [CrossRef]
12. Pei, X.; Gan, L.; Tong, Z.; Gao, H.; Meng, S.; Zhang, W.; Wang, P.; Chen, Y. Robust cellulose-based composite adsorption membrane for heavy metal removal. *J. Hazard. Mater.* **2021**, *406*, 124746. [CrossRef] [PubMed]
13. Ianăși, C.; Ianăși, P.; Negrea, A.; Ciopec, M.; Ivankov, O.I.; Kuklin, A.I.; Almásy, L.; Putz, A.-M. Effects of catalysts on structural and adsorptive properties of iron oxide-silica nanocomposites. *Korean J. Chem. Eng.* **2021**, *38*, 292–305. [CrossRef]
14. Putz, A.-M.; Ciopec, M.; Negrea, A.; Grad, O.; Ianăși, C.; Ivankov, O.I.; Milanovic, M.; Stijepovic, I.; Almásy, L. Comparison of Structure and Adsorption Properties of Mesoporous Silica Functionalized with Aminopropyl Groups by the Co-Condensation and the Post Grafting Methods. *Materials* **2021**, *14*, 628. [CrossRef] [PubMed]
15. Guevara-Lora, I.; Wronski, N.; Bialas, A.; Osip, H.; Czosnek, C. Efficient Adsorption of Chromium Ions from Aqueous Solutions by Plant-Derived Silica. *Molecules* **2022**, *27*, 4171. [CrossRef]
16. Zhao, G.; Jiang, L.; He, Y.; Li, J.; Dong, H.; Wang, X.; Hu, W. Sulfonated graphene for persistent aromatic pollutant management. *Adv. Mater.* **2011**, *23*, 3959–3963. [CrossRef]
17. Li, J.; Duan, Q.; Wu, Z.; Li, X.; Chen, C. Few-layered metal-organic framework nanosheets as a highly selective and efficient scavenger for heavy metal pollution treatment. *Chem. Eng. J.* **2019**, *383*, 123189. [CrossRef]
18. Novoselov, K.; Geim, A.; Morozov, S.; Jiang, D.; Zhang, Y.; Dubonos, S.; Grigorieva, I.; Firsov, A. Electric field effect in atomically thin carbon films. *Science* **2004**, *306*, 666–669. [CrossRef]
19. Viana, M.; Amparo, S.; Lima, M.; Lopes, R.; Silva, G. Microwave-assisted synthesis of polyacrylamide-aminated graphene oxide hybrid hydrogel with improved adsorption properties. *J. Environ. Chem. Eng.* **2020**, *8*, 104415. [CrossRef]
20. Zhao, Z.; Bai, P.; Du, W.; Liu, B.; Guo, Z. An Overview of Graphene and Its Derivatives Reinforced Metal Matrix Composites: Preparation, Properties and Applications. *Carbon* **2020**, *170*, 302–326. [CrossRef]
21. Safaviyan, M.; Faramarzi, M.; Parsa, S.; Karimi, H. Tetraethylenepentamine-enriched magnetic graphene oxide as a novel Cr (VI) removal adsorbent. *React. Funct. Polym.* **2022**, *180*, 105410. [CrossRef]
22. Boulanger, N.; Kuzenkova, A.; Iakunkov, A.; Romanchuk, A.; Trigub, A.; Egorov, A.; Bauters, S.; Amidani, L.; Retegan, M.; Kvashnina, K.; et al. Enhanced Sorption of Radionuclides by Defect-Rich Graphene Oxide. *ACS Appl. Mater. Interfaces* **2020**, *12*, 45122–45135. [CrossRef]
23. Bao, S.; Liu, H.; Liu, Y.; Yang, W.; Li, K. Amino-functionalized graphene oxide-supported networked Pd–Ag nanowires as highly efficient catalyst for reducing Cr(VI) in industrial effluent by formic acid. *Chemosphere* **2020**, *257*, 127245. [CrossRef] [PubMed]
24. Han, X.; Liu, Y.; Xiong, L.; Huang, H.; Zhang, Q.; Li, L.; Yu, X.; Wei, L. Facile assembly of polyaniline/graphene oxide composite hydrogels as adsorbent for Cr(VI) removal. *Polym. Compos.* **2019**, *40*, E1777–E1785. [CrossRef]
25. Huang, M.; Xie, L.; Wang, Y.; Feng, X.; Gao, J.; Lou, Z.; Xiong, Y. Efficient and selective capture of uranium by polyethyleneimine-modified chitosan composite microspheres from radioactive nuclear waste. *Environ. Pollut.* **2023**, *316*, 120550. [CrossRef] [PubMed]
26. Xue, F.; He, H.; Zhou, H.; Quan, Z.; Chen, Z.; Wu, Q.; Zhu, H.; Wang, S. Structural design of a cellulose-based hyperbranched adsorbent for the rapid and complete removal of Cr(VI) from water. *Chem. Eng. J.* **2021**, *417*, 128037. [CrossRef]

27. Park, S.H.; Shin, S.; Park, C.H.; Jeon, S.; Gwon, J.; Lee, S.Y.; Kim, S.J.; Kim, H.J.; Lee, J.H. Poly(acryloyl hydrazide)-grafted cellulose nanocrystal adsorbents with an excellent Cr(VI) adsorption capacity. *J. Hazard. Mater.* **2020**, *394*, 122512. [CrossRef]
28. Wang, J.; Zhao, L.; Duan, W.; Han, L.; Chen, Y. Adsorption of aqueous Cr (VI) by novel fibrous adsorbent with amino and quaternary ammonium groups. *Ind. Eng. Chem. Res.* **2012**, *51*, 13655–13662. [CrossRef]
29. Lin, C.; Wang, X.; Hu, E.; Yang, Q.; Zhang, Q.; Zhu, A.; Liu, Q. Quaternized triblock polymer anion exchange membranes with enhanced alkaline stability. *J. Membr. Sci.* **2017**, *541*, 358–366.
30. Gao, Q.; Keller, A. Novel disinfection method for toxic cyanobacteria (*Oscillatoria tenuis*) and simultaneous removal of cyanotoxins aided by recyclable magnetic nanoparticles. *J. Environ. Chem. Eng.* **2021**, *9*, 106589. [CrossRef]
31. Ragheb, E.; Shamsipur, M.; Jalali, F.; Mousavi, F. Modified magnetic-metal organic framework as a green and efficient adsorbent for removal of heavy metals. *J. Environ. Chem. Eng.* **2022**, *10*, 107297. [CrossRef]
32. Mak, S.; Chen, D. Fast adsorption of methylene blue on polyacrylic acid-bound iron oxide magnetic nanoparticles. *Dyes. Pigm.* **2004**, *61*, 93–98. [CrossRef]
33. Chang, Y.; Chen, D. Preparation and adsorption properties of monodisperse chitosan-bound Fe_3O_4 magnetic nanoparticles for removal of Cu (II) ions. *J. Colloid Interf. Sci.* **2005**, *283*, 446–451. [CrossRef]
34. Hummers, W., Jr.; Offeman, R. Preparation of graphitic oxide. *J. Am. Chem. Soc.* **1958**, *80*, 1339. [CrossRef]
35. Liao, M.; Chen, D. Preparation and characterization of a novel magnetic nano-adsorbent. *J. Mater. Chem.* **2002**, *12*, 3654–3659. [CrossRef]
36. Li, X.; Zhu, H.; Feng, J.; Zhang, J.; Deng, X.; Zhou, B.; Zhang, H.; Xue, D.; Li, F.; Mellors, N. One-pot polylol synthesis of graphene decorated with size-and density-tunable Fe_3O_4 nanoparticles for porcine pancreatic lipase immobilization. *Carbon* **2013**, *60*, 488–497. [CrossRef]
37. Berger, C.; Song, Z.; Li, T.; Li, X.; Ogbazghi, A.Y.; Feng, R.; Dai, Z.; Marchenkov, A.N.; Conrad, E.H.; First, P.N. Ultrathin epitaxial graphite: 2D electron gas properties and a route toward graphene-based nanoelectronics. *J. Phys. Chem. B* **2004**, *108*, 19912–19916. [CrossRef]
38. Liu, M.; Wen, T.; Wu, X.; Chen, C.; Hu, J.; Li, J.; Wang, X. Synthesis of porous Fe_3O_4 hollow microspheres/graphene oxide composite for Cr (VI) removal. *Dalton Trans.* **2013**, *42*, 14710–14717. [CrossRef] [PubMed]
39. Bao, S.; Yang, W.; Wang, Y.; Yu, Y.; Sun, Y. Highly efficient and ultrafast removal of Cr(VI) in aqueous solution to ppb level by poly(allylamine hydrochloride) covalently cross-linked amino-modified graphene oxide. *J. Hazard. Mater.* **2021**, *409*, 124470. [CrossRef]
40. Wu, Y.; Jiang, G.; Cano, Z.P.; Liu, G.; Liu, W.; Feng, K.; Lui, G.; Zhang, Z.; Chen, Z. Highly efficient removal of suspended solid pollutants from wastewater by magnetic Fe_3O_4-graphene oxides nanocomposite. *ChemistrySelect* **2018**, *3*, 11643–11648. [CrossRef]
41. He, Y.; Xiao, W.; Li, G.; Yang, F.; Wu, P.; Yang, T.; Chen, C.; Ding, P. A novel lead-ion-imprinted magnetic biosorbent: Preparation, optimization and characterization. *Environ. Technol.* **2017**, *40*, 1397762. [CrossRef] [PubMed]
42. Bouazizi, N.; Vieillard, J.; Bargougui, R.; Couvrat, N.; Thoumire, O.; Morin, S.; Ladam, G.; Mofaddel, N.; Brun, N.; Azzouz, A.; et al. Entrapment and stability of iron nanoparticles within APTES modified graphene oxide sheets with improved catalytic activity. *J. Alloys Compd.* **2019**, *771*, 1090–1102. [CrossRef]
43. Tran, H.V.; Tran, T.L.; Le, T.D.; Le, T.D.; Nguyen, H.M.T.; Dang, L.T. Graphene oxide enhanced adsorption capacity of chitosan/magnetite nanocomposite for Cr(VI) removal from aqueous solution. *Mater. Res. Express* **2018**, *6*, 25018. [CrossRef]
44. Sravanthi, K.; Ayodhya, D.; Swamy, P. Eco-friendly synthesis and characterization of phytogenic zero-valent iron nanoparticles for efficient removal of Cr(VI) from contaminated water. *Emergent Mater.* **2019**, *2*, 327–335. [CrossRef]
45. Liu, X.; Liu, Y.; Zhang, T. Preparation of magnetic zeolite/chitosan composite using silane as modifier for adsorption of Cr(VI) from aqueous solutions. *J. Vinyl. Addit. Technol.* **2021**, *27*, 640–654. [CrossRef]
46. Zhang, H.; Ma, R.; Yang, Y.; Huang, L.; Chen, N.; Xie, Q. Study of ion-imprinted adsorbent materials on diatom-based Cr(VI) Surfaces. *Mater. Lett.* **2022**, *308*, 131149. [CrossRef]
47. Jia, W.; Du, J.; Jiang, M.; Zhang, M.; Han, E.; Niu, H.; Wu, D. Preparation and Cr (VI) adsorption of functionalized polyimide fibers. *J. Appl. Polym. Sci.* **2022**, *139*, e52799. [CrossRef]
48. Chen, G.; Li, H.; Yang, X.; Wen, J.; Pang, Q.; Zhang, J. Adsorption of 3d transition metal atoms on graphene-like gallium nitride monolayer: A first-principles study. *Superlattices Microstruct.* **2018**, *115*, 108–115. [CrossRef]
49. Tan, L.; Zhang, X.; Liu, Q.; Jing, X.; Liu, J.; Song, D.; Hu, S.; Liu, L.; Wang, J. Synthesis of Fe_3O_4@ TiO_2 core–shell magnetic composites for highly efficient sorption of uranium (VI). *Colloids Surf.* **2015**, *469*, 279–286. [CrossRef]